

NANO EXPRESS

Open Access



# Carbon Nanodots as Dual-Mode Nanosensors for Selective Detection of Hydrogen Peroxide

Cheng-Long Shen<sup>1</sup>, Li-Xia Su<sup>1</sup>, Jin-Hao Zang<sup>1</sup>, Xin-Jian Li<sup>1</sup>, Qing Lou<sup>1\*</sup>  and Chong-Xin Shan<sup>1,2\*</sup>

## Abstract

Hydrogen peroxide ( $H_2O_2$ ) is an important product of oxidase-based enzymatic reactions, such as glucose/glucose oxidase (GOD) reaction. Therefore, the probing of generated  $H_2O_2$  for achieving the detection of various carbohydrates and their oxidases is very significative. Herein, we report one kind of dual-emission carbon nanodots (CDs) that can serve as novel dual-mode nanosensors with both fluorometric and colorimetric output for the selective detection of  $H_2O_2$ . The dual-model nanosensors are established only by the undecorated dual-emission CDs, where significant fluorometric and colorimetric changes are observed with the addition of different concentrations of  $H_2O_2$  in the CD solution, which benefit to the achievement of the naked-eye detection for  $H_2O_2$ . The mechanism of the nanosensors can be attributed to the fact that the external chemical stimuli like hydroxyl radicals from  $H_2O_2$  bring about the change of surface properties and the aggregation of CDs, which dominate the emission and absorption of CDs. The constructed dual-mode nanosensors exhibit good biocompatibility and high selectivity toward  $H_2O_2$  with a linear detection range spanning from 0.05 to 0.5 M and allow the detection of  $H_2O_2$  as low as 14 mM.

**Keywords:** Carbon nanodots, Fluorescence, Dual-mode nanosensors, Detection

## Background

Fluorescent carbon nanodots (CDs) have triggered extensive research attention for their unique physicochemical properties like good biocompatibility, low toxicity, tunable photoluminescence (PL), and high quantum yield. Because of the above characters, CDs have found potential applications in a variety of fields including but not limited to bioimaging, biosensors, and light-emitting devices [1–9]. Moreover, due to their up-conversion and down-conversion ability, lack of optical blinking, and high photostability compared to organic dyes or semiconductor quantum dots (QDs), CDs are more suitable for applications in fluorescent nanosensors by fluorescence increase or quenching [10–19].

Hydrogen peroxide ( $H_2O_2$ ) is one kind of common oxidizer, which is always used as medical disinfectant for the ability of sterilization. Besides,  $H_2O_2$  is also an

important product of oxidase-based enzymatic reactions, such as glucose/glucose oxidase (GOD) reaction. Therefore, the sensing strategy through the probing of  $H_2O_2$  can be employed as a promising approach for the detection of carbohydrates and their oxidases. For this reason, the sensing of  $H_2O_2$  may be used to monitor the diseases about carbohydrate metabolism, such as diabetes. Currently, although various glucose sensors based on the determination of  $H_2O_2$  have been developed by using a variety of analytical methods, previously reported sensor systems are mainly based on a single signal such as conductometric, fluorometric, or colorimetric change [20–22]. Recently, advances in nanotechnology, especially in fluorescent nanoparticles like semiconductor QDs and emerging carbon-based nanoparticles have brought about novel  $H_2O_2$  nanosensors. Lu et al. developed one kind of dual-emission microhybrids (DEMBs) by combining CdTe QDs and rhodamine for ratiometric fluorescent sensing of glucose through monitoring the generation of  $H_2O_2$  [20]. Zhang et al. reported a fluorescent nanosensor that showed selective and sensitive

\* Correspondence: louqing19861020@qq.com; cxshan@zzu.edu.cn

<sup>1</sup>School of Physics and Engineering, Zhengzhou University, No. 75 Daxue Road, Zhengzhou 450052, China

Full list of author information is available at the end of the article

response to  $\text{H}_2\text{O}_2$  through the fluorescence quenching of CDs [21, 22]. However, these work inevitably brought about the intrinsic defects of semiconductor-based QDs with expensive chemical constituents and heavy metal pollution. Moreover, the nanosensors based on single signal readout, either fluorescence quenching or color change, may have poor assay stability due to the fluctuations of environmental factors and the experimental operation errors. On account of the above consideration, we wish to develop a new class of fluorescent CDs, whose fluorescence and solution color are very sensitive to the change of the concentrations of  $\text{H}_2\text{O}_2$ . Thus, a dual-mode nanosensor based on these CDs can be achieved for distinctively and sensitively sensing the  $\text{H}_2\text{O}_2$  by simultaneously inspecting the fluorometric and colorimetric changes of CD solution, which is beneficial to the realization of naked-eye detection of the  $\text{H}_2\text{O}_2$ .

In this study, we have developed a facile and convenient method to synthesize a novel type of CDs, which exhibits a dark red solution color under visible light and dual fluorescent emission under a 365-nm UV lamp (blue and green fluorescence emission). The CDs are simply synthesized through solvothermal method with citric acid, urea, and *N,N*-dimethylformamide (DMF) as carbon source, nitrogen source, and reaction solvent, respectively. The fluorescence and solution color are very sensitive to changes in the concentrations of  $\text{H}_2\text{O}_2$ . Thus, a dual-mode nanosensor based on these CDs can be achieved for distinctively and sensitively sensing the  $\text{H}_2\text{O}_2$  by simultaneously inspecting the fluorometric and colorimetric changes of the CD solution, which is beneficial to the realization of naked-eye detection of the  $\text{H}_2\text{O}_2$ . Without the introduction of any expensive instrument, a dual-mode nanosensor based on these CDs has been established. This sensing system may effectively avoid the potential operation errors and markedly improve the reliability of the measurement. In addition, the CD-based nanosensors are promising in the application of blood glucose detection both in vivo and in vitro owing to their good biocompatibility and high water solubility.

## Methods

### Synthesis of CDs

The CDs were prepared using a solvothermal method with citric acid as the carbon source, urea as the nitrogen source, and DMF as the co-reactant. In a typical experiment, citric acid (1 g) and urea (2 g) were dissolved in 10 mL DMF. The solution was then transferred to a 25-mL poly(tetrafluoroethylene)-lined autoclave and heated at 160 °C for 4 h. After the reaction, the autoclave was naturally cooled down to room temperature. A dark red solution was obtained.

The CDs were precipitated by adding 5 mL reaction solution into 25 mL abundant ethanol and centrifuged at 7500 rpm for 30 min. Then, the precipitation was dialyzed to obtain pure CDs. The as-prepared CDs were collected and dried in a vacuum drying oven at 60 °C and under <1 Pa for 12 h. Then, the CDs were redissolved in deionized water to form 0.75 mg mL<sup>-1</sup> CD solution for further research. And the subsequent  $\text{H}_2\text{O}_2$ -treated CDs were collected and dried with the same method for the characterization of the surface morphology and structural properties.

### Measurements

The surface morphology of the CDs was characterized by a high-resolution transmission electron microscope (HRTEM, JEOL JSM-IT100). The structural properties of the CDs were performed by an X-ray diffractometer (XRD, PA National X'Pert Pro) and a micro-Raman spectrometer (Renishaw RM 2000). The absorption spectra of the CDs were measured on a Hitachi U-3900 UV-Vis-NIR spectrophotometer. The fluorescence spectra of the CDs were measured by a spectrophotometer (Hitachi F-7000). The fluorescence quantum yield of the CDs was obtained by the Horiba FL-322 spectrometer with a calibrated integrating sphere. The fluorescence decay curves of the CDs were also measured by Horiba FL-322 using a 405-nm NanoLED monitoring the emission at 450 and 500 nm, respectively. The Fourier transform infrared spectrum (FTIR) of the CDs was recorded on a Bio-Rad Excalibur spectrometer (Bruker Vector 22). X-ray photoelectron spectroscopy (XPS) was recorded on an ESCALAB MK II X-ray photoelectron spectrometer using Mg as the exciting source.

### Establishment of the CD Nanosensors

For the detection of the  $\text{H}_2\text{O}_2$ , the fluorescence and absorption spectra of the CDs in the presence of  $\text{H}_2\text{O}_2$  were examined in PBS buffer (pH = 7.4, at 25 °C). In a typical experiment, a different amount of  $\text{H}_2\text{O}_2$  was mixed with distilled water firstly and then 20  $\mu\text{L}$  0.75 mg mL<sup>-1</sup> CD solution was injected into 4 mL  $\text{H}_2\text{O}_2$  solution with different concentrations (0, 0.05, 0.1, 0.15, 0.25, 0.5, 1.0, and 2.0 M). Then, photographs, fluorescence, and absorption spectra were taken after the CDs were added into the  $\text{H}_2\text{O}_2$  solution.

The selectivity of the CD-based nanosensors was also evaluated. The CD solution (20  $\mu\text{L}$ , 3.75  $\mu\text{g mL}^{-1}$ ) was mixed with different kinds of cations and oxidants (4 mL, 0.1 M) and then the solution was shaken for 1 min. At last, the UV-Vis absorption and fluorescence spectra of the solution were recorded after the CDs were added into the  $\text{H}_2\text{O}_2$  solution.

## Results and Discussion

### Characterization of the CDs

The morphology of the as-prepared CDs was measured by transmission electron microscope (TEM). As shown in Fig. 1a, the CDs are well dispersed with a uniform size range of 2.5–6.5 nm and an average diameter of around 5 nm (Additional file 1: Figure S1b). Moreover, the HRTEM image (inset of the Fig. 1a) shows the diffraction fringes around 0.21 nm which agrees with the (100) of graphite. The XRD patterns of the CDs shown in Fig. 1b exhibit a broad peak at around  $23.4^\circ$ , which is corresponding to the highly disordered carbon atoms with a graphite-like carbon structure. The Raman spectra of the CDs (Fig. 1c) reveal two bands: D band (at around  $1347\text{ cm}^{-1}$ , which was due to the vibrations of  $\text{sp}^3$ -

hybridized carbon with imperfection and disorder) and G band (at around  $1577\text{ cm}^{-1}$ , which was associated with the  $E_{2g}$  vibration modes of  $\text{sp}^2$ -hybridized carbon in a two-dimensional hexagonal crystalline structure). The FTIR spectra of the CDs (Fig. 1d) present broad vibration absorption bands of O–H/N–H at  $3100\text{--}3600\text{ cm}^{-1}$ , the stretching vibrations of C=O/C=C at around  $1690\text{--}1610\text{ cm}^{-1}$  and the stretching vibrations of N–O at around  $1350\text{--}1390\text{ cm}^{-1}$ . The above data indicate that there may be some functional groups on the surface of the CDs, and these functional groups may play an important role in the high hydrophilicity and stability of the CDs in aqueous solution.

The fluorescent behavior of the CD-based nanosensors toward  $\text{H}_2\text{O}_2$  was measured in the CD aqueous solutions

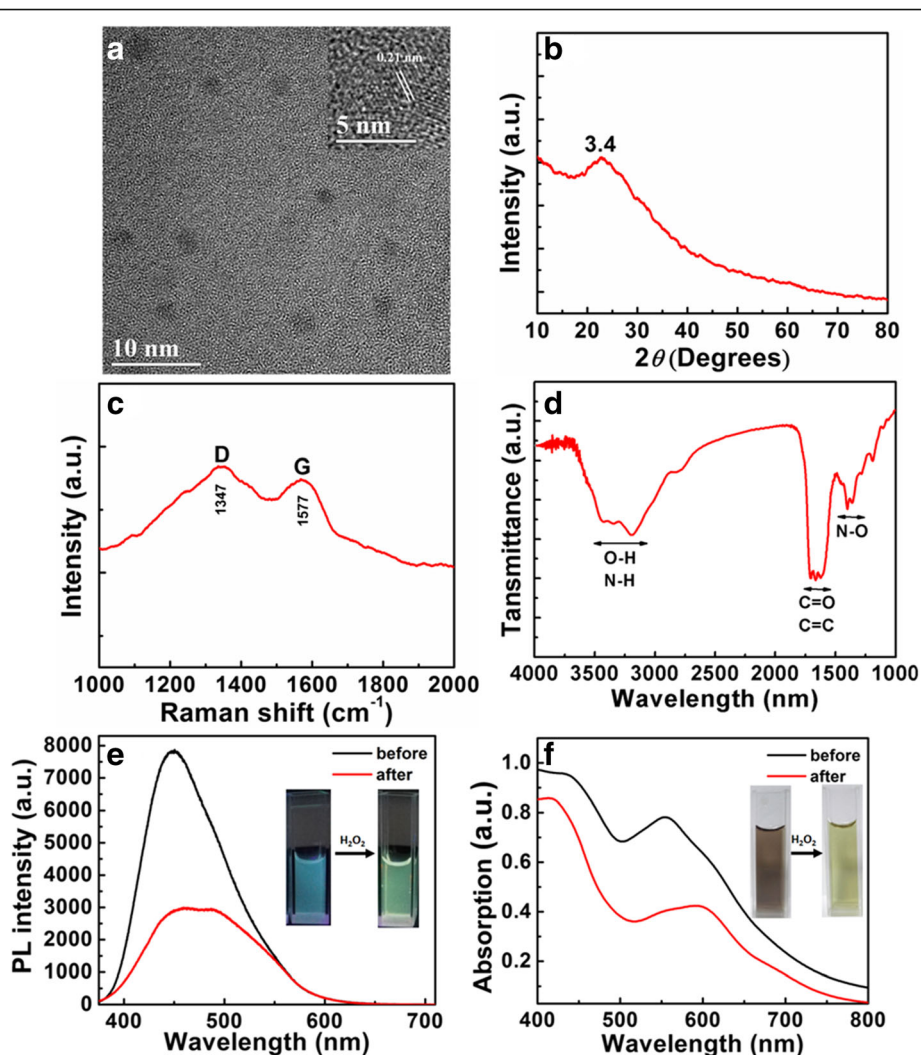


**Fig. 1** **a** TEM image of the CDs. *Insets* show the HRTEM image of the CDs. **b** XRD pattern of the CDs. **c** Raman spectroscopy of the CDs. **d** FTIR spectroscopy of the CDs. **e** Fluorescence variation of CDs after adding 0.5 M  $\text{H}_2\text{O}_2$ . *Insets* show photographs of CDs before (*left*) and after (*right*) adding the  $\text{H}_2\text{O}_2$  under UV light. **f** Colorimetric variation of CDs after adding 0.5 M  $\text{H}_2\text{O}_2$ . *Insets* show photographs of CDs before (*left*) and after (*right*) adding the  $\text{H}_2\text{O}_2$  under daylight

shown in Fig. 1e. Under a single wavelength excitation at 365 nm, the CD solutions illustrate asymmetrical emission spectra, which could be fitted by dual-emission fluorescent bands centered at 450 and 500 nm, corresponding to blue and green fluorescent bands, respectively. When the CD solutions are mixed with  $\text{H}_2\text{O}_2$ , the intensity of the blue band demonstrates a greater decrease than that of the green one. Accordingly, the strongest emissions of the CDs shift from 450 to 500 nm from the results of the excitation-emission matrices of the CDs after the addition of the  $\text{H}_2\text{O}_2$  (Additional file 1: Figure S2). As a result, the fluorescence color of the CD solutions changes from blue to green under a 365-nm UV lamp illumination (inset of the Fig. 1e). Moreover, the CD solutions simultaneously experience a colorimetric change from dark red to green after adding the  $\text{H}_2\text{O}_2$  (inset of the Fig. 1f). This color change can be attributed to the intensity evolution of the absorption bands at around 555 and 595 nm caused by the addition of  $\text{H}_2\text{O}_2$  in the CD solution (Fig. 1f). Taken together, these results confirm the CDs could be used as a dual-mode nanosensor for the detection of  $\text{H}_2\text{O}_2$ .

### Sensing Mechanism

To investigate the sensing mechanism, the morphology and fluorescence properties of the CDs after adding  $\text{H}_2\text{O}_2$  were also characterized. As illustrated in

Additional file 1: Figures S1a and S1c, the addition of  $\text{H}_2\text{O}_2$  into the CD solution can lead to the aggregation of CDs, whose sizes are ranging from 30 to 60 nm. The  $\text{H}_2\text{O}_2$ -induced aggregation of CDs was also revealed in the normalized absorption spectra (Additional file 1: Figure S3); namely, the absorption band of the CDs redshifts from 555 to 595 nm in the visible region [15]. Correspondingly, the color of the CD solution varies from dark red to green, along with the dispersion state of CDs turning into an aggregation state. The XRD spectra (Fig. 1b and Additional file 1: Figure S4) of the CDs before and after adding  $\text{H}_2\text{O}_2$  alter little, indicating there are no changes in the crystalline structure of the CDs.

The fluorescence evolution of the as-prepared CDs with the addition of  $\text{H}_2\text{O}_2$  was investigated by fluorescence spectra. The excitation-emission matrices show that the addition of  $\text{H}_2\text{O}_2$  makes the emission centers of the CDs change from 450 to 500 nm (Additional file 1: Figure S2). The fluorescence decay curves shown in Fig. 2a for the CDs with the emission at 450 and 500 nm can be well fitted by a mono-exponential decay function with an average lifetime of 7.96 and 7.12 ns, respectively (under excitation of 365 nm). In contrast, the fluorescence decay lifetime of the CDs after the  $\text{H}_2\text{O}_2$  treatment turned into 4.53 and 4.83 ns (Fig. 2b and Table 1). Meanwhile, the PL quantum yield ( $\eta_{\text{int}}$ ) of CDs changed from 5.5 to 4.6% when the  $\text{H}_2\text{O}_2$  was added in the CD

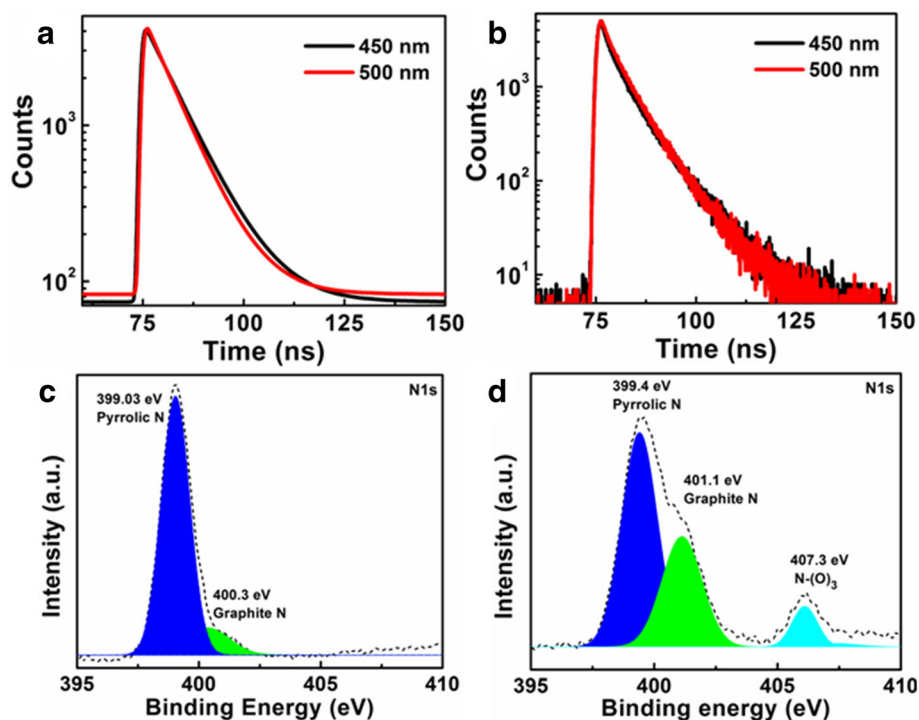


**Fig. 2** a, b Fluorescence decay of CDs before (a) and after (b) adding 0.5 M  $\text{H}_2\text{O}_2$ . c, d XPS (N1s) of CDs before (c) and after (d) adding 0.5 M  $\text{H}_2\text{O}_2$

**Table 1** Photophysical data for CDs ( $3.75 \mu\text{g mL}^{-1}$  in deionized water) before and after 0.5 M  $\text{H}_2\text{O}_2$  treatment

States	$\lambda_{\text{em}}^{\text{a}}$ (nm)	$\tau^{\text{b}}$ (ns)	$\chi^2^{\text{c}}$	QY <sup>d</sup> (%)
Before	450	7.96	0.999	5.5
Before	500	7.12	0.999	
After	450	4.53	0.993	4.6
After	500	4.83	0.996	

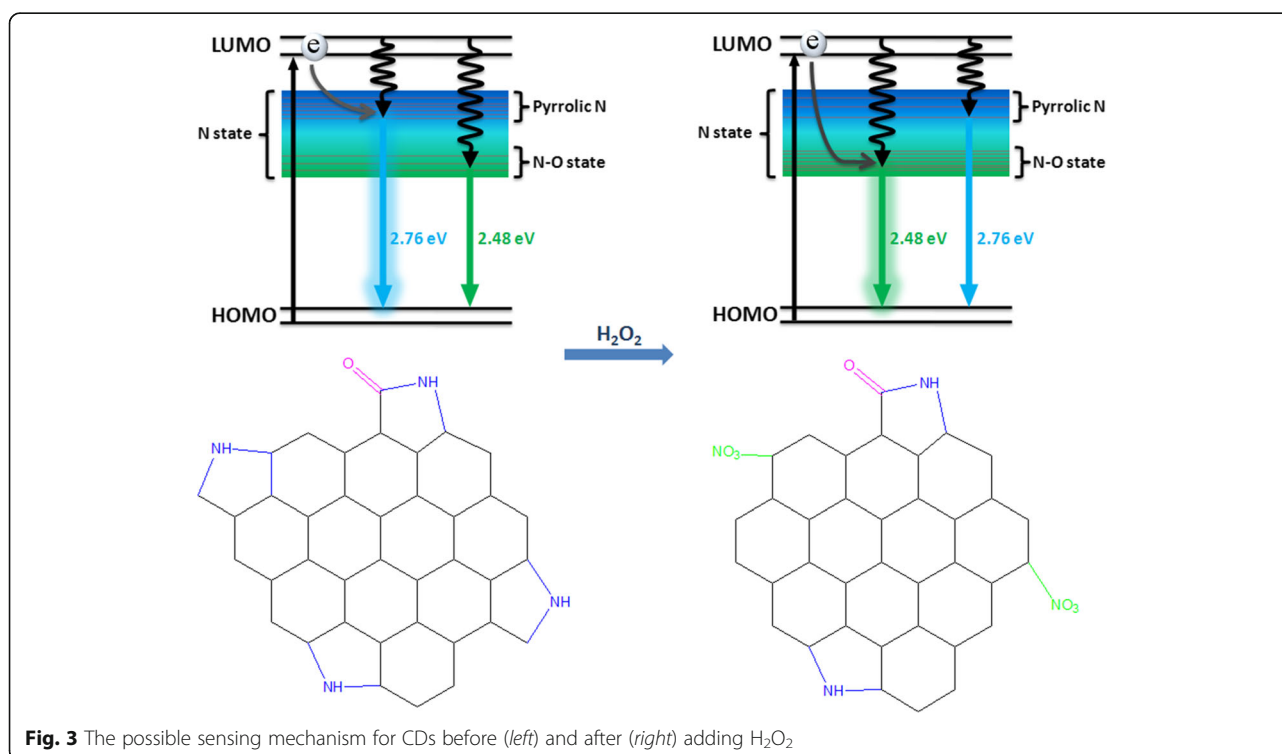
<sup>a</sup>PL peak excited at 405 nm<sup>b</sup>PL lifetime<sup>c</sup>Goodness of fit<sup>d</sup>PL quantum yield excited at 365 nm

solution. Considering the change of fluorescence lifetime and PL quantum yield, it can be concluded that charge transfer (CT) may occur between CDs and  $\text{H}_2\text{O}_2$ , which could be a trigger to make the change of PL spectra of the CDs.

The FTIR and XPS spectra of the CDs were measured to give insight into the chemical composition and environmental changes caused by the  $\text{H}_2\text{O}_2$ . The FTIR spectra of CDs before and after adding  $\text{H}_2\text{O}_2$  shown in Additional file 1: Figure S7 illustrate that the stretching vibrations of N–O at around  $1350\text{--}1390 \text{ cm}^{-1}$  increase with the addition of  $\text{H}_2\text{O}_2$ , which is also confirmed by the result of the XPS spectra. It is observed from the full survey XPS spectra (Additional file 1: Figure S8) that the O to N ratio of the CDs before and after the  $\text{H}_2\text{O}_2$  treatment was 1.57 and 3.85, respectively. The increasing ratio of O/N reveals that the bonding states of N in the

CDs may change with the addition of the  $\text{H}_2\text{O}_2$ , which is in line with the high-resolution N1s XPS spectra shown in Fig. 2c, d. From the result of the N1s XPS spectra, the content of graphite N in the CDs has been increased with the addition of the  $\text{H}_2\text{O}_2$ . Furthermore, there is an additional peak of N–O state at 407.3 eV in the N1s spectra after the addition of the  $\text{H}_2\text{O}_2$ , which obviously demonstrates that the importing of the  $\text{H}_2\text{O}_2$  brings about the variation of the surface states in the CDs. All the surveys manifest that the surface N frame could be changed by the addition of the  $\text{H}_2\text{O}_2$ .

Previous reports suggest that the emission bands of the CDs are related to the surface states such as N-doped radicals and urea groups [5, 9, 12, 23–25]. Meanwhile, these surface states are sensitive to external physical or chemical stimuli. On the basis of the photophysical and surface environmental analysis, we propose the mechanism of the fluorescence evolution with the introduction of the  $\text{H}_2\text{O}_2$  (Fig. 3). The edge state of the as-prepared CDs is consisted of the conjugated pyrrolic N groups. This type of N state may be mostly localized at high energy level. Thus, the excited electron may non-radiatively relax to the high-level surface N state and then radiatively transfer to ground state accompanied with fluorescence emission bands around 450 nm. In contrast, the fluorescence intensity of the CD solution slightly decreases because of the dynamic quenching between the  $\text{H}_2\text{O}_2$  and the CDs, where the CT arises between CDs and  $\text{H}_2\text{O}_2$  similar to the previous reports



[26–29]. Otherwise, it could be deduced that the high-energy fluorescence radicals (related N state) are transformed into the lower-energy N–O state in virtue of the impact of hydroxyl radical from the  $\text{H}_2\text{O}_2$ . So, the excited electron may mostly relax with a radiative transition from the lower-energy N–O state to ground state with a green emission band at 500 nm, which also results in the static quenching of 450-nm fluorescence. Therefore, the major emission bands of CDs could present a change from the blue emission to the green emission.

#### Evaluation of the CDs Nanosensors

On the basis of the above fluorescent and colorimetric behavior of the CDs, we have developed a nanosensor to detect  $\text{H}_2\text{O}_2$  by the CDs. The proposed sensing system is consisted of CDs with proper concentration in aqueous solution ( $3.75 \mu\text{g mL}^{-1}$ , Additional file 1: Figure S9), where the CDs serve dual function as both colorimetric and fluorometric reporters in this system.

The proposed nanosensing system based on the CD solution is illustrated in Fig. 4. The fluorometric and

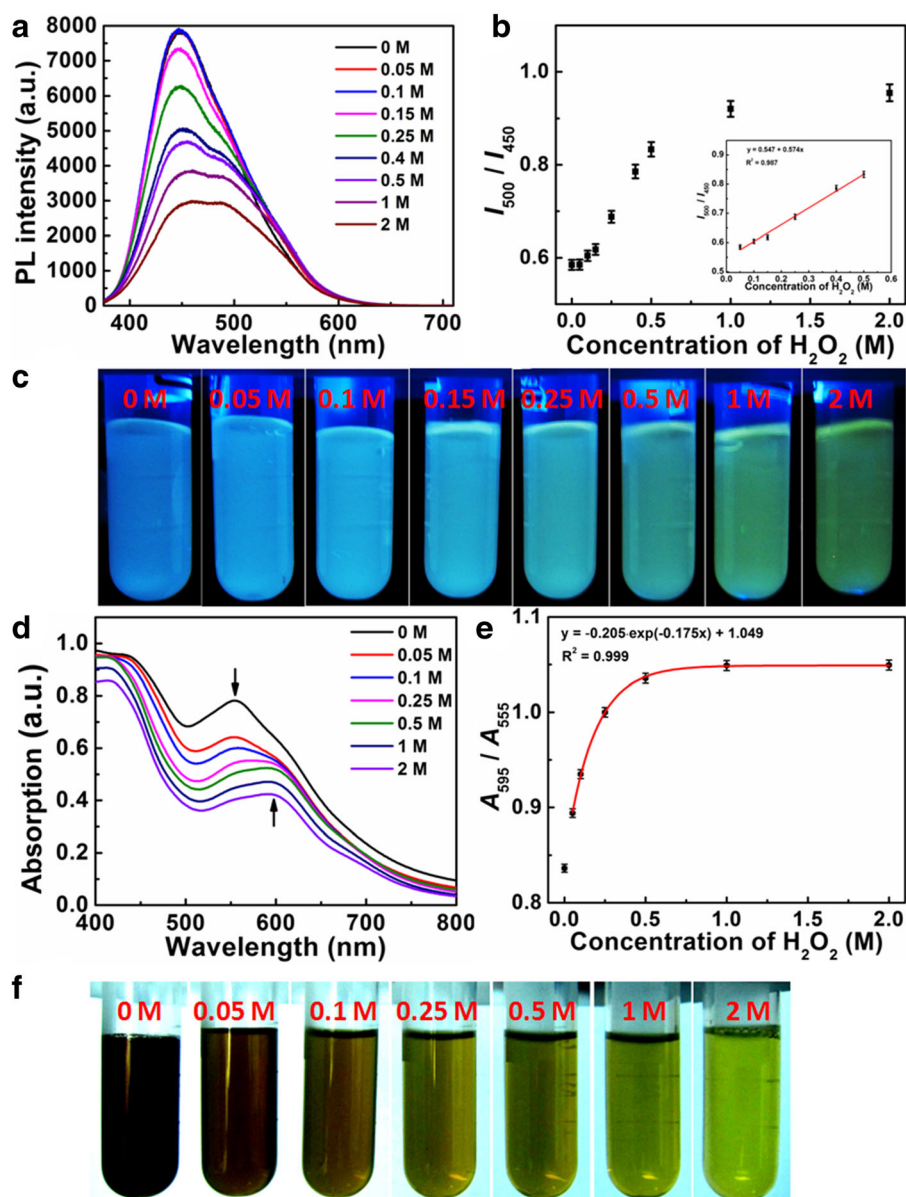


**Fig. 4** **a** Fluorescence spectra of CDs in the presence of different  $\text{H}_2\text{O}_2$  concentrations. **b** Calibration curve of  $I_{500}/I_{450}$  of the CDs vs.  $\text{H}_2\text{O}_2$  concentration. *Inset*s show the linear detection range of  $I_{500}/I_{450}$  of the CDs vs.  $\text{H}_2\text{O}_2$  concentration. **c** Photographic images of the fluorescence CD solution under different concentrations of  $\text{H}_2\text{O}_2$ . **d** UV-Vis spectra of CDs in the presence of different  $\text{H}_2\text{O}_2$  concentrations. **e** Calibration curve of  $A_{595}/A_{555}$  of the CDs vs.  $\text{H}_2\text{O}_2$  concentration. **f** Photographic images of the CD solution under different concentrations of  $\text{H}_2\text{O}_2$

colorimetric change caused by  $\text{H}_2\text{O}_2$  could be distinctly visualized by the naked eye (Fig. 4c, f), where a series of noticeable color change from blue to green and from dark red to green can be observed under UV light and daylight illumination. Besides, the addition of  $\text{H}_2\text{O}_2$  into the CD solution can also be expressed quantitatively with the fluorescence and absorption spectra (Fig. 4a, d). As shown in Fig. 4a, the fluorescence band centered at 450 and 500 nm decreases gradually with the increase of the  $\text{H}_2\text{O}_2$  concentration from 0 to 2 M. However, the increase of the  $\text{H}_2\text{O}_2$  concentration leads to the different decrease of fluorescence intensity at 450 nm ( $I_{450}$ ) and 500 nm ( $I_{500}$ ), which accords well with the fluorescence color change in the CD solution (Fig. 4c). Therefore, the ratio of the fluorescence intensity at 500 nm to that at 450 nm is selected to monitor the  $\text{H}_2\text{O}_2$  concentration (Fig. 4a, b). The lower ratio is related to the blue emission, while the green fluorescence can be observed by the naked eyes at a higher ratio of  $I_{500}$  to  $I_{450}$ . The linear detection range by these means spans from 0.05 to 0.5 M with a linear correlation  $R^2 = 0.987$ . Similarly, the colorimetric change occurs in the CD solution on account of the inhomogeneous decrease of the absorption band at 555 and 595 nm. As displayed in Fig. 4d, the absorption intensity decreases in the visible region, but the increase of the  $\text{H}_2\text{O}_2$  concentration results in that the absorption around 595 nm decreases more slowly than around 555 nm. Hence, the ratio of the absorption at 595 nm ( $A_{595}$ ) to that at 555 nm ( $A_{555}$ ) could be also used to measure the  $\text{H}_2\text{O}_2$  concentration. The ratio of  $A_{595}$  to  $A_{555}$  increases exponentially from 0.05 to 2 M with an exponential correlation  $R^2 = 0.999$ , and the colorimetric change correlates well to the  $\text{H}_2\text{O}_2$  concentration range from 0.05 to 0.25 M with the linear detection limit (LOD) of 14 mM (Additional file 1: Figure S11 and Table S1). The dual-mode nanosensors have a proper sensitivity of this method satisfying the clinical and medicinal requirements due to the concentration of  $\text{H}_2\text{O}_2$  through the GOD reaction ranging around millimolar ( $\sim 10$  mM) in plasma [20]. In addition, the dual-mode nanosensors have an intrinsic built-in calibration reference, so intensity fluctuation and other externally caused factors can be eliminated, which contributes to the promotion of the testing accuracy.

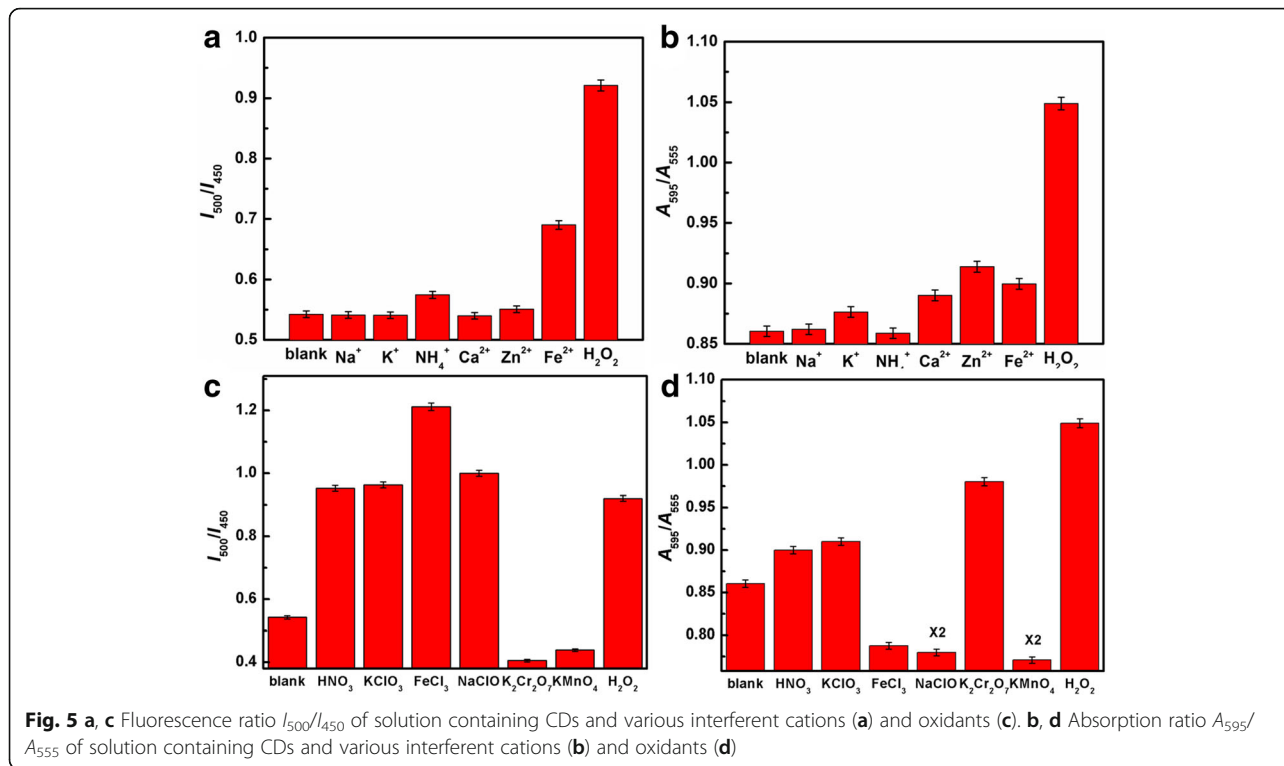
To evaluate the selectivity of the nanosensors toward  $\text{H}_2\text{O}_2$ , interference assays were performed under identical conditions using some common cations, such as  $\text{Na}^+$ ,  $\text{K}^+$ ,  $\text{NH}_4^+$ ,  $\text{Ca}^{2+}$ ,  $\text{Zn}^{2+}$ , and  $\text{Fe}^{2+}$ . As shown in Fig. 5a, b, the fluorometric and colorimetric changes of the CDs have been surveyed in the presence of different cations. In the presence of  $\text{Na}^+$ ,  $\text{K}^+$ ,

$\text{NH}_4^+$ ,  $\text{Ca}^{2+}$ ,  $\text{Zn}^{2+}$ , and  $\text{Fe}^{2+}$ , the fluorescence ratio of  $I_{500}$  to  $I_{450}$  and the absorption ratio of  $A_{595}$  to  $A_{555}$  appear only as a slight variation compared with the blank sample, which mean these cations have little interference on the detection of  $\text{H}_2\text{O}_2$ . Moreover, we have also compared the impact on the CDs with other oxidants, such as  $\text{HNO}_3$ ,  $\text{KClO}_3$ ,  $\text{FeCl}_3$ ,  $\text{NaClO}$ ,  $\text{K}_2\text{Cr}_2\text{O}_7$ , and  $\text{KMnO}_4$  (Fig. 5c, d and Additional file 1: Figures S12 and S13), and we found that the fluorescence color changes from blue to green with the addition of these oxidants except  $\text{K}_2\text{Cr}_2\text{O}_7$  and  $\text{KMnO}_4$ . So, we can rule out the interference from  $\text{K}_2\text{Cr}_2\text{O}_7$  and  $\text{KMnO}_4$  through the fluorescence change. In addition, we can easily exclude the impact from other oxidants like  $\text{HNO}_3$ ,  $\text{KClO}_3$ ,  $\text{FeCl}_3$ , and  $\text{NaClO}$  from the result of the absorption ratio of  $A_{595}$  to  $A_{555}$ . Hence, the dual-mode nanosensors demonstrated in this paper may be very promising in the high selectivity of the determination due to the synergistic effect of the two independent detection methods [30–33]. Furthermore, we have measured the response time of the fluorometric change upon the addition of  $\text{H}_2\text{O}_2$  and found that the fluorescence decreases after injecting  $\text{H}_2\text{O}_2$  and is kept stable at about 3.3 s (Additional file 1: Figure S14).

The viability of A549 cell was examined using standard CCK-8 assay for assessing the cytotoxicity of CDs. As shown in Fig. 6, we find that near 80% viability is obtained by incubating the A549 cells with CDs for 48 h even at high concentration of CDs like  $500 \mu\text{g mL}^{-1}$ . It is calculated that the 50% inhibitive concentration (IC50) of CDs is about  $1106 \mu\text{g mL}^{-1}$  by the GraphPad Prism 5.0, which deduces the CDs have good biocompatibility and very low cytotoxicity at high concentration. Moreover, we have compared the analytical performance of previously reported nanosensors for the  $\text{H}_2\text{O}_2$  determination shown in Additional file 1: Table S2. The biocompatibility, simplicity, and visualization of the detection are comparable to or even better than most of these reported  $\text{H}_2\text{O}_2$  assays. Considering that the CD-based dual-mode nanosensors have a good selectivity toward  $\text{H}_2\text{O}_2$  detection, the proper detection limit (LOD = 14 mM) at the same order with the blood glucose, and very low cytotoxicity at high concentration of CDs, the nanosensors are promising to be used in the test of blood glucose and other clinical requirements.

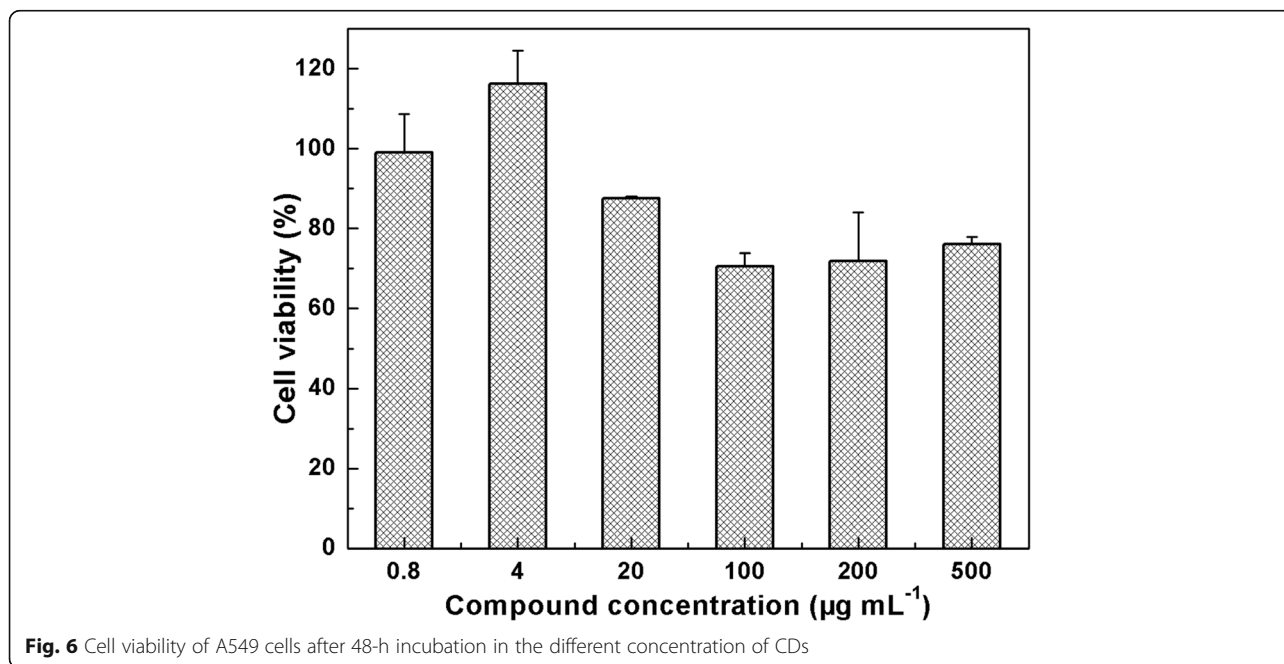
## Conclusions

In conclusion, we propose a dual-mode nanosensor based on CDs with both colorimetric and fluorometric output for the quantitative detection of  $\text{H}_2\text{O}_2$  based on the fluorometric and colorimetric change of the CD solution upon the introduction of  $\text{H}_2\text{O}_2$ . The nanosensors are



simple and facile to achieve naked-eye detection for H<sub>2</sub>O<sub>2</sub>. The mechanism of the nanosensors can be attributed to the fact that the external chemical stimuli like hydroxyl radicals from H<sub>2</sub>O<sub>2</sub> bring about the change of surface properties and the aggregation of CDs, which dominate the emission and absorption of CDs. The proposed nanosensors exhibit good biocompatibility, high selectivity

toward H<sub>2</sub>O<sub>2</sub> with a linear detection range spanning from 0.05 to 0.5 M, and a detection limit of around 14 mM, which is comparable to the level of H<sub>2</sub>O<sub>2</sub> produced by the GOD reactions. It is believed that the strategy reported in this paper may provide a promising approach for developing a novel sensor in blood glucose, which could be valuable in disease diagnosis and environmental testing.



## Additional file

**Additional file 1: Fig. S1.** (a) TEM image of CDs after adding 0.5 M H<sub>2</sub>O<sub>2</sub>. (b,c) Histogram of distribution from TEM before (b) and (c) after adding 0.5 M H<sub>2</sub>O<sub>2</sub>. **Fig. S2.** Excited-emission matrix of the CDs with 2500 rpm (a), 5000 rpm(b), 7500 rpm(c) centrifugation and with the addition in 0.5 M H<sub>2</sub>O<sub>2</sub> (d). **Fig. S3.** Absorption spectrum of the CDs normalized at 500 nm before and after adding 0.5 M H<sub>2</sub>O<sub>2</sub>. **Fig. S4.** XRD pattern of the CDs after adding 0.5 M H<sub>2</sub>O<sub>2</sub>. **Fig. S5.** Raman spectrum of the CDs after adding 0.5 M H<sub>2</sub>O<sub>2</sub>. **Fig. S6.** (a) Fluorescence stability of the CDs before and after adding 0.5 M H<sub>2</sub>O<sub>2</sub> with the emission at 450 nm and 500 nm, respectively. (b) Photographic images of the CDs and the CDs under 1M H<sub>2</sub>O<sub>2</sub> after 3 day. **Fig. S7.** FTIR spectra of the CDs before and after adding 0.5 M H<sub>2</sub>O<sub>2</sub>. **Fig. S8.** (a,b) XPS (full survey) of the CDs before (a) and after (b) adding 0.5 M H<sub>2</sub>O<sub>2</sub>. (c,d) XPS (C1s) of CDs before (c) and after (d) adding 0.5 M H<sub>2</sub>O<sub>2</sub>. (e,f) XPS (O1s) of CDs before (e) and after (f) adding 0.5 M H<sub>2</sub>O<sub>2</sub>. **Fig. S9.** The fluorescence intensity of the 112.5 μg mL<sup>-1</sup> CDs diluted for 10, 20, 30 and 40 times. **Fig. S10.** The normalized fluorescence intensity of the CDs under different concentrations of H<sub>2</sub>O<sub>2</sub> (0, 0.05, 0.1, 0.15, 0.25, 0.5, 1 and 2 M, from left to right). **Fig. S11.** The liner range of the absorption for sensing H<sub>2</sub>O<sub>2</sub>. **Fig. S12.** Fluorescence spectra of CDs in the presence of different oxidants. **Fig. S13.** UV-vis spectra of CDs in the presence of different oxidants. **Fig. S14.** The fluorescence intensity varied with time after injecting H<sub>2</sub>O<sub>2</sub>. **Tab. S1.** Limit of detection (LOD) of CDs sensor for H<sub>2</sub>O<sub>2</sub>. **Tab. S2.** Comparison of analytical performance of different nanosensors for H<sub>2</sub>O<sub>2</sub> determination. (PDF 1384 kb)

## Acknowledgements

This work is financially supported by the National Science Foundation for Distinguished Young Scholars of China (61425021); the National Natural Science Foundation of China (51602288, 11374296, and 51272238); China Postdoctoral Science Foundation (2015M582192 and 2016T90671); and Startup Research Fund of Zhengzhou University (1512317006).

## Authors' Contributions

CXS conceived the idea and supervised the project. CLS and QL designed and conducted the experiments. CLS, LXS, QL, CXS, and JHZ performed the data analysis. CLS, QL, JHZ, CXS, and XJL wrote the manuscript. All of the authors discussed the manuscript. All the authors read and approved the final manuscript.

## Competing Interests

The authors declare that they have no competing interests.

## Publisher's Note

Springer Nature remains neutral with regard to jurisdictional claims in published maps and institutional affiliations.

## Author details

<sup>1</sup>School of Physics and Engineering, Zhengzhou University, No. 75 Daxue Road, Zhengzhou 450052, China. <sup>2</sup>State Key Laboratory of Luminescence and Applications, Changchun Institute of Optics, Fine Mechanics and Physics, Chinese Academy of Sciences, No. 3888 Dong Nanhu Road, Changchun 130033, China.

Received: 26 March 2017 Accepted: 26 June 2017

Published online: 06 July 2017

## References

- Georgakilas V, Perman JA, Tucek J, Zboril R (2015) Broad family of carbon nanoallotropes: classification, chemistry, and applications of fullerenes, carbon dots, nanotubes, graphene, nanodiamonds, and combined superstructures. *Chem Rev* 115(11):4744–4822
- Wang H, Gao P, Wang Y, Guo J, Zhang K, Du D, Dai X, Zou G (2015) Fluorescently tuned nitrogen-doped carbon dots from carbon source with different content of carboxyl groups. *APL Mater* 3(8):086102
- Li Y, Zhang L, Huang J, Liang R, Qiu J (2013) Fluorescent graphene quantum dots with a boronic acid appended bipyridinium salt to sense monosaccharides in aqueous solution. *Chem Commun* 49(45):5180–5182
- Teng P, Xie J, Long Y, Huang X, Zhu R, Wang X, Liang L, Huang Y, Zheng H (2014) Chemiluminescence behavior of the carbon dots and the reduced state carbon dots. *J Lumin* 146(1):464–469
- Dong Y, Cai J, You X, Chi Y (2015) Sensing applications of luminescent carbon based dots. *Analyst* 140(22):7468–7486
- Qu S, Wang X, Lu Q, Liu X, Wang L (2012) A biocompatible fluorescent ink based on water-soluble luminescent carbon nanodots. *Angew Chem Int Edit* 51(49):12215–12218
- Qian ZS, Shan XY, Chai LJ, Ma JJ, Chen JR, Feng H (2014) A universal fluorescence sensing strategy based on biocompatible graphene quantum dots and graphene oxide for the detection of DNA. *Nanoscale* 6(11):5671–5674
- Zhu L, Cui X, Wu J, Wang Z, Wang P (2014) Fluorescence immunoassay based on carbon dots as labels for the detection of human immunoglobulin G. *Anal Methods* 6(12):4430–4436
- Zhang H, Chen Y, Liang M, Xu L, Qi S, Chen H, Chen X (2014) Solid-phase synthesis of highly fluorescent nitrogen-doped carbon dots for sensitive and selective probing ferric ions in living cells. *Anal Chem* 86(19):9846–9852
- Lu S, Cong R, Zhu S, Zhao X, Liu J, S Tse J, Meng S, Yang B (2016) pH-dependent synthesis of novel structure-controllable polymer-carbon nanodots with high acidophilic luminescence and super carbon dots assembly for white light-emitting diodes. *ACS Appl Mater Inter* 8(6):4062–4068
- Ong W, Tan L, Ng YH, Yong S, Chai S (2016) Graphitic carbon nitride (g-C<sub>3</sub>N<sub>4</sub>)-based photocatalysts for artificial photosynthesis and environmental remediation: are we a step closer to achieving sustainability? *Chem Rev* 116(12):7159–7329
- Liu J, Liu Y, Liu N, Han Y, Zhang X, Huang H, Lifshitz Y, Lee ST, Zhong J, Kang Z (2015) Metal-free efficient photocatalyst for stable visible water splitting via a two-electron pathway. *Science* 347(6225):970–974
- Wang Y, Zhang L, Liang R, Bai J, Qiu J (2013) Using graphene quantum dots as photoluminescent probes for protein kinase sensing. *Anal Chem* 85(19):9148–9155
- Dong Y, Wang R, Li H, Shao J, Chi Y, Lin X, Chen G (2012) Polyamine-functionalized carbon quantum dots for chemical sensing. *Carbon* 50(8):2810–2815
- Shi Y, Pan Y, Zhang H, Zhang Z, Li M, Yi C, Yang M (2014) A dual-mode nanosensor based on carbon quantum dots and gold nanoparticles for discriminative detection of glutathione in human plasma. *Biosens Bioelectron* 56(3):39–45
- Guan Y, Qu S, Li B, Zhang L, Ma H, Zhang L (2016) Ratiometric fluorescent nanosensors for selective detecting cysteine with upconversion luminescence. *Biosens Bioelectron* 77:124–130
- Li X, Zhu S, Xu B, Ma K, Zhang J, Yang B, Tian W (2013) Self-assembled graphene quantum dots induced by cytochrome C: a novel biosensor for trypsin with remarkable fluorescence enhancement. *Nanoscale* 5(17):7776–7779
- Song Z, Quan F, Xu Y, Liu M, Cui L, Liu J (2016) Multifunctional N,S co-doped carbon quantum dots with pH- and thermo-dependent switchable fluorescent properties and highly selective detection of glutathione. *Carbon* 104:169–78
- Qu S, Chen H, Zheng X, Cao J, Liu X (2013) Ratiometric fluorescent nanosensor based on water soluble carbon nanodots with multiple sensing capacities. *Nanoscale* 5(12):5514–5518
- Lu X, Wang P, Wang Y, Liu C, Li Z (2016) A versatile dual-emission fluorescent microhybrid enabling visual detection of glucose and other oxidases-based biocatalytic systems. *Adv Mat Technol*. doi:10.1002/admt.201600024
- Zhang Y, Yang X, Gao Z (2015) In situ polymerization of aniline on carbon quantum dots: a new platform for ultrasensitive detection of glucose and hydrogen peroxide. *RSC Adv* 5(28):21675–21680
- Feng L, Liang F, Wang Y, Xu M, Wang X (2011) A highly sensitive water-soluble system to sense glucose in aqueous solution. *Org Biomol Chem* 9(8):2938–2942
- Qu S, Zhou D, Li D, Ji W, Jing P, Han D, Liu L, Zeng H, Shen D (2016) Toward efficient orange emissive carbon nanodots through conjugated sp<sup>2</sup>-domain controlling and surface charges engineering. *Adv Mater* 28(18):3516–3521
- Qu D, Zheng M, Du P, Zhou Y, Zhang L, Li D, Tan H, Zhao Z, Xie Z, Sun Z (2013) Highly luminescent S, N co-doped graphene quantum dots with

- broad visible absorption bands for visible light photocatalysts. *Nanoscale* 5(24):12272–12277
25. Mu Y, Wang N, Sun Z, Wang J, Li J, Yu J (2016) Carbogenic nanodots derived from organo-templated zeolites with modulated full-color luminescence. *Chem Sci* 7(6):3564–3568
  26. Li H, Sun C, Vijayaraghavan R, Zhou F, Zhang X, MacFarlane DR (2016) Long lifetime photoluminescence in N, S co-doped carbon quantum dots from an ionic liquid and their applications in ultrasensitive detection of pesticides. *Carbon* 104:33–39
  27. Campos BB, Contreras-Cáceres R, Bandoz TJ, Jiménez-Jiménez J, Rodríguez-Castellón E, Esteves Da Silva JCG, Algarra M (2016) Carbon dots as fluorescent sensor for detection of explosive nitrocompounds. *Carbon* 106: 171–178
  28. Delehanty JB, Susumu K, Manthe RL, Algar WR, Medintz IL (2012) Active cellular sensing with quantum dots: transitioning from research tool to reality; a review. *Anal Chim Acta* 750(11):63–81
  29. Qu D, Zheng M, Li J, Xie Z, Sun Z (2015) Tailoring color emissions from N-doped graphene quantum dots for bioimaging applications. *Light-Sci Appl* 4(12):364
  30. Dong Y, Cai J, Fang Q, You X, Chi Y (2016) Dual-emission of lanthanide metal-organic frameworks encapsulating carbon based dots for ratiometric detection of water in organic solvents. *Anal Chem* 88(3): 1748–1752
  31. Yu C, Wu Y, Zeng F, Wu S (2013) A fluorescent ratiometric nanosensor for detecting NO in aqueous media and imaging exogenous and endogenous NO in live cells. *J Mater Chem B* 1(33):4152–4159
  32. Li L, Wu G, Yang G, Peng J, Zhao J, Zhu JJ (2013) Focusing on luminescent graphene quantum dots: current status and future perspectives. *Nanoscale* 5(10):4015–4039
  33. Cheng L, Wang C, Liu Z (2013) Upconversion nanoparticles and their composite nanostructures for biomedical imaging and cancer therapy. *Nanoscale* 5(1):23–37

**Submit your manuscript to a SpringerOpen<sup>®</sup> journal and benefit from:**

- Convenient online submission
- Rigorous peer review
- Open access: articles freely available online
- High visibility within the field
- Retaining the copyright to your article

---

Submit your next manuscript at ► [springeropen.com](http://springeropen.com)

---